JOURNAL OF GEOPHYSICAL RESEARCH, VOL. 99, NO. D8, PAGES 17,001–17,020, AUGUST 20, 1994

# Radiative-convective model with an explicit hydrologic cycle 2. Sensitivity to large changes in solar forcing

Nilton O. Rennó,[1] Peter H. Stone, and Kerry A. Emanuel

Center for Meteorology and Physical Oceanography, Massachusetts Institute of Technology, Cambridge

**Abstract.** The one-dimensional radiative-convective equilibrium model with an explicit hydrologic cycle introduced in part 1 is used to study the sensitivity of the model's atmosphere to large changes in the solar forcing, when various cumulus convection parameterizations are used. As shown by Simpson [1927], by Komabayasi [1967], and by Ingersoll [1969] when the concentration of the absorbing gas in the atmosphere is temperature dependent, equilibrium is impossible for values of the solar forcing larger than a critical value. This result is referred to as a runaway greenhouse. The cumulus convection parameterization schemes currently in use in global climate models (GCMs) employ different assumptions about moistening. This causes the critical solar forcing above which a runaway greenhouse occurs to be very sensitive to the cumulus convection scheme employed. Furthermore, using the microphysically based cumulus convection scheme proposed by Emanuel [1991], we show that the sensitivity of the equilibrium temperature to changes in the solar forcing depends crucially on the microphysics of cumulus convection. For fixed cloud conditions, the critical solar forcing for a runaway greenhouse to occur is between approximately 1.22 and 1.49 times the global mean value for the Earth, and for clear sky conditions, it is a few percent lower. The runaway greenhouse in the experiments with the mass flux schemes generally occurs more rapidly than in the experiments with the adjustment schemes. In addition, the inability of the hard convective adjustment scheme to produce an efficient vertical transport of moisture, together with the saturation requirement for convection to occur, leads to the breakdown of the radiative-convective equilibria when other processes are not available to provide the necessary vertical transport of water vapor.

## 1. Introduction

One-dimensional radiative-convective models are very useful for understanding the heat budget of planetary atmospheres. Their main value is that they allow one to examine general principles and test fundamental ideas. Their major drawback is the inability to compute the feedbacks between the horizontal heat transports and the temperature structure from first principles. In spite of the inability of these one-dimensional models to compute the horizontal transports, multidimensional models (e.g., global climate models (GCMs)) are not yet clearly superior for studying global climate change. This is apparent from the large errors in GCM simulations of atmospheric transports, which are very sensitive to the sub-grid-scale physics [*Stone and Risbey,* 1990]. It is also apparent from the large artificial sources of heat and moisture that coupled atmosphere-ocean GCMs need to simulate the current climate [*Manabe et al.,* 1991]. The main drawback of the previous climate studies with radiative-convective models is the fact that they did not include the hydrologic cycle; instead, the atmosphere's water vapor mixing ratio was diagnosed based on the climatological profile of relative humidity [*Manabe and Strickler,* 1964; *Sarachik,* 1978; *Lindzen*

[1] Now at Lawrence Livermore National Laboratory, Livermore, California.



Paper number 94JD01332.
0148-0227/94/94JD-01332$05.00

*et al.*, 1982]. The exception to this rule is the model of *Betts and Ridgway* [1988] in which the water vapor vertical distribution was computed through a mixing line assumption [*Betts*, 1982, 1985], but here too, the water vapor profile is severely constrained by climatology. Thus in general, previous models used very simple numerical procedures to parameterize cumulus convection. Since water vapor is the most important greenhouse gas and its content and vertical distribution in the atmosphere is to a large extent controlled by moist convection, it is desirable to explicitly compute the atmospheric water vapor content.

In the present work we use a radiative-convective equilibrium model which explicitly includes a hydrologic cycle [*Rennó*, 1992; *Rennó et al.*, 1994], to study the sensitivities of radiative-convective equilibria to large changes in the solar forcing. In this model, cumulus convection is parameterized by a variety of complex schemes, similar to those used in GCMs. The following cumulus convection parameterization schemes are compared: the moist convective adjustment (MCA) scheme [*Manabe et al.*, 1965], the Kuo scheme [*Kuo*, 1974], the early GISS Model (GISS1) scheme [*Arakawa*, 1969; *Somerville et al.*, 1974], the GISS Model II (GISS2) scheme [*Hansen et al.*, 1983], and the Emanuel scheme [*Emanuel*, 1991]. We use two versions of the MCA scheme, one is in the form originally proposed by *Manabe et al.* [1965], hereafter referred to as the hard convective adjustment (HCA) scheme, while the other is the soft convective adjustment (SCA) scheme. In the SCA scheme it is assumed that only a fraction of the convecting grid is covered by convection.

As shown by *Simpson* [1927] and by *Komabayasi* [1967], for a grey gas, and by *Ingersoll* [1969], for a gas in which the absorption coefficient is a function of the infrared wavelength, when the concentration of the absorbing gas in the atmosphere is temperature dependent, equilibrium is impossible for values of the solar forcing larger than a critical one, thus resulting in a runaway greenhouse. The cumulus convection parameterization schemes currently in use in GCMs employ different assumptions about moistening. We will show in the present work that this causes the critical solar forcing above which a runaway greenhouse occurs to be very sensitive to the cumulus convection scheme employed. Furthermore, using the microphysically based cumulus convection scheme of *Emanuel* [1991], we show that the critical solar forcing above which runaway greenhouse occurs depends crucially on the microphysics of cumulus convection.

In part 1 [*Rennó et al.*, 1994] we showed that a good understanding of the essential physics governing the water vapor transport by cumulus convection is crucial in climate simulations. Here, in part 2, we explore the model sensitivities to large changes in the solar forcing and the breakdown of the radiative-convective equilibrium, i.e. the runaway greenhouse. In Part 3 we will explore the sensitivities of the radiative-convective equilibria to $CO_2$ doubling and to small changes in the solar forcing.

## 2. Description of the Model

### 2.1. Model Equations

The model's basic equations are

$$\frac{\partial \theta}{\partial t} = Q + R + F_\theta, \tag{1}$$

$$\frac{\partial r}{\partial t} = C + F_r. \tag{2}$$

Independent variables are time, $t$, and pressure, $p$. The prognostic variables are the potential temperature, $\theta$, and the water vapor mixing ratio, $r$. $Q$ in equation (1) represents the diabatic heating by cumulus convection and large-scale condensation and $C$ in equation (2) stands for the moisture source. These terms are computed by the cumulus convection scheme and represent the net effects of cumulus convection. $R$ in equation (1) represents the net radiative heating. Radiation is computed by a sophisticated parameterization scheme [*Chou*, 1992; *Chou et al.*, 1991], described in the next subsection. The model integrations were started from the mean sounding of GATE phase III.

Vertical diffusion of temperature and moisture are parameterized by the Fickian law. We present results of experiments with values of diffusion coefficients equal to 2 $m^2$ $s^{-1}$. This small diffusion is not supposed to represent any real physical process, but it is included for numerical convenience. The observed eddies are represented by the parameterized convection.

We use centered differences in the vertical direction. Time integration of the nondiffusive terms is performed by the leapfrog scheme with an Asselin filter [*Asselin*, 1972] inserted at every time step to damp its computational mode. The smoothing constant of the Asselin filter is set at 0.1. The time integration of the diffusive terms is performed by the Euler forward scheme. The time step is set to 15 min and radiative fluxes are computed each 12 hours. Cumulus convection and large-scale condensation are computed every time step. Experiments are made with the number of vertical layers equal to 16 in the model's troposphere. The thickness of these vertical layers is constant in pressure. The troposphere's top is at 40 mbar and the model's surface is at 1000 mbar. Above the model's troposphere, there is an upper layer extending from 40 to 1 mbar, in radiative equilibrium. This upper layer is subdivided into 10 sub-layers for the computation of the radiative fluxes.

Since the main role of the ocean in the radiative-convective equilibrium is to be wet (we are interested in the equilibrium solution), we use a "swamp" as the lower boundary. The "swamp" is a saturated surface in which the heat capacity is zero and the supply of moisture is infinite. Therefore the net energy flux into the surface is required to be zero at each instant. This is not

exactly true in our model, since for numerical stability we set the "swamp" temperature equal to the averaged temperature computed in the preceding 96 time steps (24 hours).

Surface fluxes are computed by the bulk aerodynamic formulae. The drag coefficient is set at 0.0025, the wind speed at the anemometer level at 5 m $s^{-1}$, and the surface temperature is computed by the "swamp" formulation. The atmosphere's potential temperature and the water vapor mixing ratio are made constant from the model's lowest level down to the surface. The surface pressure is fixed at 1000 mbar.

### 2.2. Radiation Model

We use a fast radiation parameterization scheme developed by *Chou* [1992] and *Chou et al.* [1991]. This scheme uses several broadband parameterization schemes for longwave and shortwave radiation in combination to produce a computationally fast and accurate radiation parameterization scheme.

Clouds are assumed to be black to infrared radiation, except for high cloud which is assumed to be half black. Each cloud type is assumed to be a separate column with no overlaps. The radiation calculations just linearly weight the flux obtained in each one of the single columns. The fraction, vertical distribution, and shortwave optical properties of the clouds used in the experiments with cloud cover are shown in Table 1. The cloud distribution is adapted from satellite observations. The parameter $\tau$ in Table 1 is the cloud optical thickness to solar radiation.

The reference carbon dioxide concentration (330 ppm), ozone mixing ratio, and stratospheric water vapor profile are from the air force Cambridge res lab (AFCRL) standard atmosphere [*McClatchey et al.*, 1972].

### 2.3. Cumulus Convection Schemes

The hard convective adjustment (HCA) scheme [*Manabe et al.*, 1965] assumes that when the temperature lapse rate of a saturated area exceeds the moist adiabatic lapse rate, free convection within the explicit cloud is strong enough to maintain a neutral lapse rate of equivalent potential temperature.

The soft convective adjustment (SCA) scheme [*Manabe et al.*, 1965] is similar to the hard convective adjustment (HCA) scheme, except for the fact that the saturation requirement for convection to occur is relaxed and that the moist adjustment occurs over a fraction of the grid-scale area. To use the soft convective adjustment (SCA) scheme in the framework of our radiative-convective equilibrium model, we include the "drying effect" of the compensating subsidence, forced by moist convection. This modified scheme is referred to as the SCA1.5D scheme [*Rennó et al.*, 1994].

**Table 1.** Cloud Distribution and Properties Used in the Experiments With Cloud Cover.

| Cloud Type | Amount, % | Height, mbar | $\tau$ |
|---|---|---|---|
| High | 14.0 | 280 - 220 | 2.0 |
| Middle | 9.0 | 640 - 460 | 6.0 |
| Low | 30.0 | 940 - 640 | 12.0 |

These are mean values for the global atmosphere adapted from satellite observations.

The Kuo scheme [*Kuo*, 1974] assumes that cumulus convection occurring in deep layers of unstable stratification is maintained by the moisture supply due to large-scale convergence and evaporation from the surface. It also assumes that the environment is modified through mixing of cumulus and environmental air, the cumulus convective heating and moistening are directly proportional to the local excess of cloud temperature and moisture over the corresponding environmental values. Left to its own devices, the Kuo scheme will eventually saturate a one-dimensional column. Thus as discussed for the SCA1.5D, to use the Kuo scheme in the framework of our radiative-convective equilibrium model, we include the "drying effect" of the compensating subsidence, forced by moist convection. This modified scheme is referred to as the Kuo1.5D scheme [*Rennó et al.*, 1994].

The GISS1 scheme [*Somerville et al.*, 1974] is an adaptation of the three-level scheme proposed by *Arakawa* [1969]. The *Arakawa* [1969] scheme is the first version of the widely known *Arakawa and Schubert* [1974] cumulus convection parameterization scheme. In the 1969 version three types of convection can occur: middle-level convection, penetrative convection, and low-level convection. Each cloud type represents an ensemble of convective elements of small total area. Each cloud entrains environmental air through its base and through its sides and detrains cloud air at its upper level. The environment is modified by detrainment of moisture through the cloud top and compensating subsidence between the clouds. The latter both warms and dries the atmosphere. Convection occurs whenever a nonentraining parcel of air rising pseudoadiabatically from the cloud base condenses and becomes positively buoyant by the time it reaches the cloud top layer.

The GISS2 scheme [*Hansen et al.*, 1983] assumes that an undiluted plume is generated in moist convectively unstable layers and rises moist adiabatically up to its level of neutral buoyancy. The plume mass is arbitrarily chosen as half the air mass of the cloud base grid box. In our one-dimensional model we set the plume mass equal to 10% of the cloud base grid box (this assumption better simulates the behavior of the scheme in the GCM). The environment is warmed and dried by the induced subsidence and moistened by the evaporation of falling precipitation. The falling precipitation is allowed to evaporate to the extent that it saturates half of the cloud area. Below cloud base, the falling precipitation is allowed to saturate the whole cloudy area.

In the Emanuel scheme [*Emanuel*, 1991] it is assumed that the fundamental entities in cumulus convection are the sub-cloud-scale drafts rather than the cloud-scale circulations themselves. Convection occurs whenever the environment is unstable to a parcel in reversible adi-

abatic ascent from the surface. Vertical transports are accomplished by saturated updrafts and downdrafts, by a single unsaturated downdraft driven by evaporation of the falling precipitation, and by the compensating subsidence.

## 3. Runaway Greenhouse

### 3.1. Experiments With No Cloud Cover

Figure 1 shows the surface equilibrium temperature obtained with the moist convective adjustments (HCA and SCA1.5D), the Kuo1.5D, the GISS1, the GISS2, and the Emanuel schemes as a function of the solar forcing, for clear sky conditions. The runaway greenhouse is clearly indicated by the rapid increase of the surface equilibrium temperature when the solar forcing approaches a critical value, dependent on the cumulus parameterization scheme being used. The critical solar forcing is different for each one of the cumulus convection schemes tested. The HCA scheme presents the lowest critical solar forcing, 332 W $m^{-2}$; followed by the GISS1 scheme, 363 W $m^{-2}$; the Emanuel scheme, 368 W $m^{-2}$; the SCA1.5D scheme, 373 W $m^{-2}$; the GISS2 scheme, 378 W $m^{-2}$; and, finally, the Kuo1.5D scheme, 424 W $m^{-2}$. When the relative humidity profile is fixed, based on climatological values [*Manabe and Wetherald,* 1967], the runaway greenhouse is inhibited (it might occur only for a very large value of the solar forcing). However, the HCA scheme still breaks down for relatively small solar forcings. This happens because the saturation requirement for convective adjustment to occur is only rarely satisfied at the lower layers. The temperature in those layers, in turn, increases abruptly, and they depart greatly from the moist adiabat. This process is studied in detail in section 5.

For the GISS1 and the Emanuel schemes the runaway greenhouse is abrupt. It occurs more rapidly because of a positive feedback generated by the interaction of the infrared radiative fluxes with detrained water vapor at the level of neutral buoyancy (see section 5 for details). The rapidly runaway greenhouse does not occur in the experiments with the GISS2 scheme because in this scheme the mass flux is fixed. It does not occur with the HCA, SCA1.5D, and Kuo1.5D schemes, because in these schemes the moistening of the detrainment layer does not depend directly on the convective mass flux, or on the magnitude of the radiative cooling there. In the HCA and SCA1.5D schemes the moistening depends only on the temperature and moisture content throughout the unstable layers, while in the case of the Kuo1.5D scheme, it depends on surface evaporation, moisture convergence, and the relative humidity of the unstable layers.

It is interesting to note two inflection points on the surface equilibrium temperature curves obtained with the SCA1.5D, the Kuo1.5D, and the GISS2 schemes. They are due to the dominance of the negative feedback of the declining tropospheric temperature lapse rate for "intermediate" values of the solar forcing. This happens because for these values of the solar forcing, the positive water vapor feedback is reduced by the strong drying effect of the compensating subsidence. When the solar forcing is further increased, the moistening due to detrainment of cloud air dominates, and the runaway greenhouse is approached. Similar inflection points are also observed on the curves for evaporation, net solar energy absorbed, and net infrared radiation emitted by the model's atmosphere (Figures 2, 3, and 4, respectively). However, only the first inflexion point is observed on the curve for net radiation emitted by the model's atmosphere (Figure 5). This is because the rate of increase of the absorption of solar radiation overcompensates the reduction of the rate of increase of infrared radiation emitted by the model's atmosphere.

For decreasing values of the solar forcing, the atmosphere becomes colder and drier (the greenhouse effect due to water vapor becomes smaller) and its tempera-

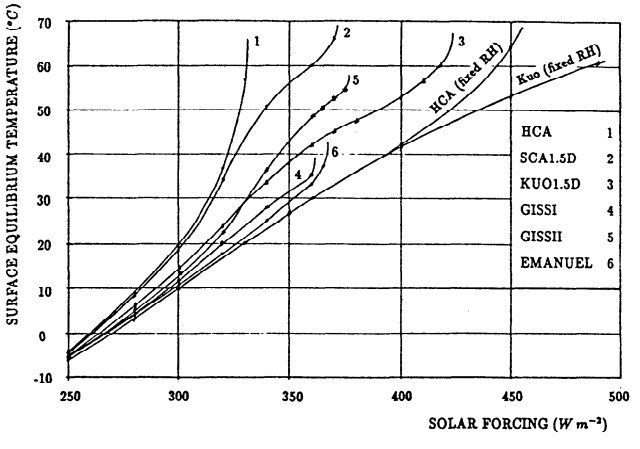


**Figure 1.** The surface temperature in radiative-convective equilibrium obtained with the various cumulus convection schemes. Clear sky conditions and interactive water vapor are assumed for the computation of the radiative fluxes, except where indicated.

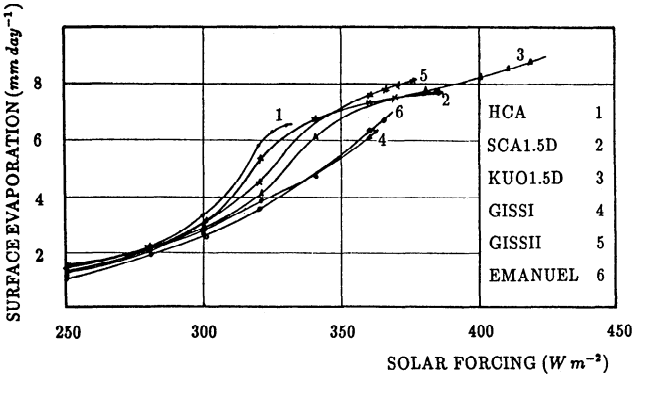


**Figure 2.** The surface evaporation rate obtained with the various cumulus convection schemes. Clear sky conditions and interactive water vapor are assumed for the computation of the radiative fluxes. Note that the evaporation in mm $day^{-1}$ multiplied by 30 approximately gives the latent heat flux in W $m^{-2}$.

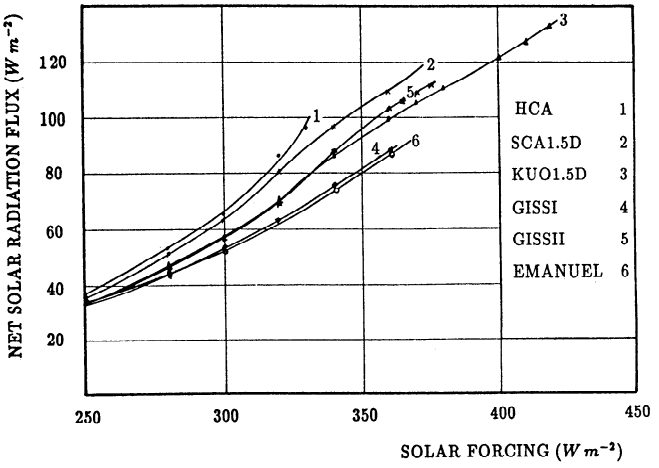


**Figure 3.** The net solar radiation flux absorbed by the model's atmosphere in radiative-convective equilibrium with the various cumulus convection schemes. Clear sky conditions and interactive water vapor are assumed for the computation of the radiative fluxes.

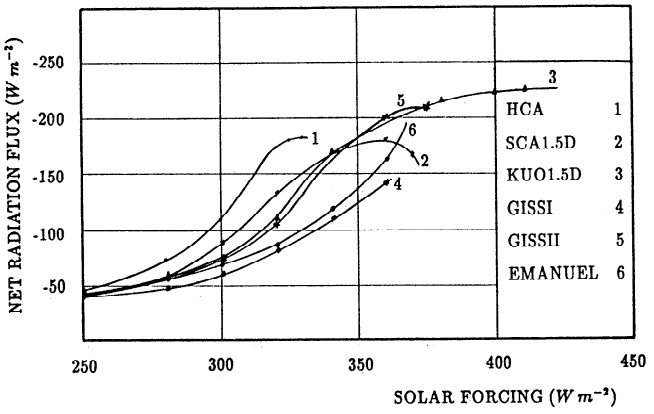


**Figure 5.** The net radiation flux throughout the model's atmosphere in radiative-convective equilibrium with the various cumulus convection schemes. Clear sky conditions and interactive water vapor are assumed for the computation of the radiative fluxes.

ture lapse rate approximates the dry adiabatic. Therefore the equilibrium solutions for all the cumulus convection schemes converge for low temperatures.

Figure 2 shows the equilibrium evaporation rate (or precipitation rate, since at equilibrium they are equal to each other) as a function of the solar forcing. The evaporation rate is very sensitive to changes in the solar forcing. Among the schemes tested, the HCA scheme presents the largest evaporation sensitivity to changes in the solar forcing, while the Emanuel and GISS1 schemes displays the smallest sensitivity. The large sensitivity of the HCA scheme is due to the large opacity of its atmosphere to infrared radiation. This large opacity leads to a small contribution of net infrared radiation in the surface heat budget. This small contribution of the net infrared radiation is compensated by increased surface evaporation. The small sensitivity of the GISS1 and Emanuel schemes is due to an opposite effect, since these schemes produce the driest atmospheres among the schemes used in this work.

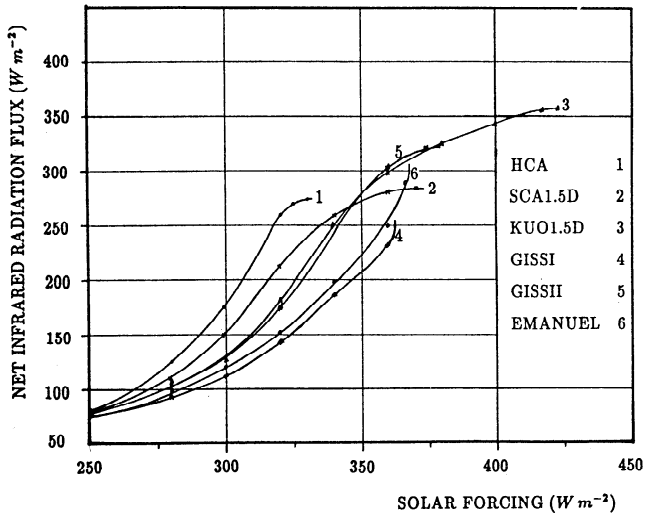


**Figure 4.** The net infrared radiation flux emitted by the model's atmosphere in radiative-convective equilibrium with the various cumulus convection schemes. Clear sky conditions and interactive water vapor are assumed for the computation of the radiative fluxes.

As mentioned above, the first inflection point noted in the curves for the equilibrium surface temperature (for the SCA1.5D, the Kuo1.5D, and the GISS2 schemes) also occurs on the curves for evaporation. This happens because in radiative-convective equilibrium the latent heat flux loosely balances the net radiative cooling of the atmosphere (since the sensible heat flux is small). Therefore the rates of increase of the atmosphere's water vapor content, net radiative cooling, and evaporation decrease. For "large" values of the solar forcing (where "large" is dependent on the cumulus convection scheme), the sensitivity of the evaporation rate to changes in the solar forcing is substantially reduced, except for the GISS1 and Emanuel schemes. This occurs because for these "large" values of the solar forcing, the rate of increase of the net atmospheric radiative cooling decreases. The reduction is due to a large increase in the atmosphere opacity. The large opacity produces both a decrease in the rate of increase of net infrared radiation emitted (Figure 4) and an increase in the amount of solar radiation absorbed by the model's atmosphere (Figure 3). This behavior is not observed in the experiments with the GISS1 and Emanuel schemes because for these schemes the runaway greenhouse occurs before the opacity of the atmosphere substantially increases (see section 5).

Figure 3 shows the net flux of solar radiation absorbed by the model's atmosphere as a function of the solar forcing. The amount of solar energy absorbed by the model's atmosphere increases with the solar forcing. This occurs because the atmospheric water vapor con-

tent increases exponentially with temperature (through the Clausius-Clapeyron equation, unless the relative humidity substantially decreases with temperature which was not observed in our model for any of the convection schemes), which in turn increases with the solar forcing. Since solar radiation is mainly absorbed by water vapor, the amount of solar energy absorbed by the atmosphere also increases with the solar forcing. The amount of solar energy absorbed by the HCA scheme, which produces a saturated atmosphere, strongly increases with the solar forcing. Inflection points are observed on the curves for the SCA1.5D, the Kuo1.5D, and the GISS2 schemes, for the same values of the solar forcing which produce inflection points in the curves for equilibrium surface temperature (Figure 1). This occurs because for values of the solar forcing between these inflection points, the strong drying effect of the compensating subsidence inhibits the moistening of the atmosphere. The reduction in the moistening rate of the atmosphere, in turn, produces a decrease in the rate of increase of the absorption of solar radiation. When the critical value of the solar forcing is reached, the large increase in the moisture content of the atmosphere produces a subtle increase in the amount of solar energy absorbed.

Figure 4 shows the net infrared radiation emitted by the model's atmosphere as a function of the solar forcing. When the solar forcing increases, the net infrared radiation flux emitted by the model's atmosphere also increases (through the increase of the atmosphere's temperature and water vapor content, i.e., of its emissivity). However, for the HCA, SCA1.5D, GISS2, and Kuo1.5D schemes the rate of increase in emitted infrared radiation decreases as the critical forcing for runaway greenhouse is approached. This happens because the atmosphere is becoming totally opaque to infrared radiation (Figure 8). Then, the rate of increase of the atmosphere's contribution to the radiation budget, at the expense of the decrease in the contribution of the surface, is decreasing rapidly. Furthermore, the emission of infrared radiation by the atmosphere is approaching the Simpson-Komabayasi-Ingersoll limit [*Simpson,* 1927; *Komabayasi,* 1967; *Ingersoll,* 1969]. At this time, more infrared radiation is emitted from upper layers (at colder temperatures) at the expense of lower layers (at warmer temperatures). This result follows from a simple solution for the absorption of radiation by the ionosphere obtained by *Chapman* [1939]. However, Chapman approximation is also valid for the emission of infrared radiation to space [*Goody and Yung,* 1989]. By assuming a constant molecular absorption coefficient and that the density of the absorber follows a barometric law, *Chapman* [1939] introduced an analytical approximation for the absorption (or emission) of radiation through a nonscattering atmosphere. According to Chapman's solution, monochromatic radiation is emitted (or absorbed) by a layer whose thickness is approximately two scale heights. The height of this absorbing layer varies with the absorption coefficient. In the framework of our radiative-convective equilibrium model, the height of the emitting layer increases with the solar forcing (Figure 6).

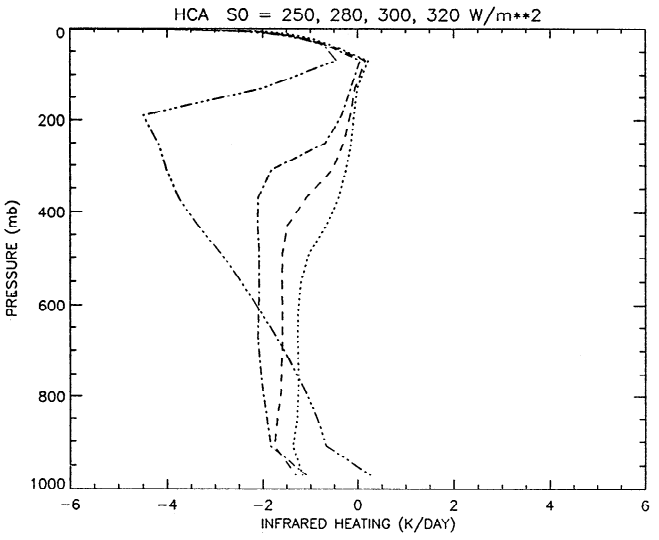


**Figure 6.** Infrared heating rate for various values of the solar forcing (250 W $m^{-2}$, dotted line; 280 W $m^{-2}$, short dashed line; 300 W $m^{-2}$, dotted-dashed line; 320 W $m^{-2}$, three-dotted-dashed line) obtained with our radiative-convective model using the hard convective adjustment (HCA) scheme. As the solar forcing is increased, more radiation is emitted from upper layers at the expense of lower layers. Also, as the Simpson-Komabayasi-Ingersoll limit is approached, the emission of radiation to space (or the heating rate) approximates the Chapman solution.

Figure 5 shows the net flux of radiation (solar plus infrared) through the model's atmosphere as a function of the solar forcing. Since the emitted infrared radiation flux is 2 to 3 times larger than the absorbed solar radiation flux, the curves for the net radiation flux throughout the model's atmosphere resembles those for the net flux of emitted infrared radiation. The HCA scheme, which produces a saturated atmosphere with a moist adiabatic temperature lapse rate (and therefore a very opaque atmosphere), also produces the strongest net emission of radiation. The GISS1 scheme produces a dry equilibrium atmosphere, with the smallest net emission of radiation among the schemes tested.

The curves in Figures 7, 8, and 9 show the response of the temperature, net infrared radiative, and net solar radiative flux profiles to increases in the solar forcing. It is interesting to note that the temperature profiles for the SCA1.5D and GISS1 schemes (Figures 7b and 7d) change their curvature in the lower troposphere as the solar forcing increases. This indicates that CAPE (convective available potential energy) increases substantially with the solar forcing. Figure 9 shows that as the solar forcing increases, more solar radiation is absorbed by the atmosphere (the flux divergence increases), especially at the upper layers. It also indicates that the rate of increase in the absorption of solar radiation is larger for the GISS1 and Emanuel schemes, which produce larger rates of increase in the atmosphere's moisture content. Finally, Figure 8 shows that with the exception of the experiments with the GISS1 and Emanuel

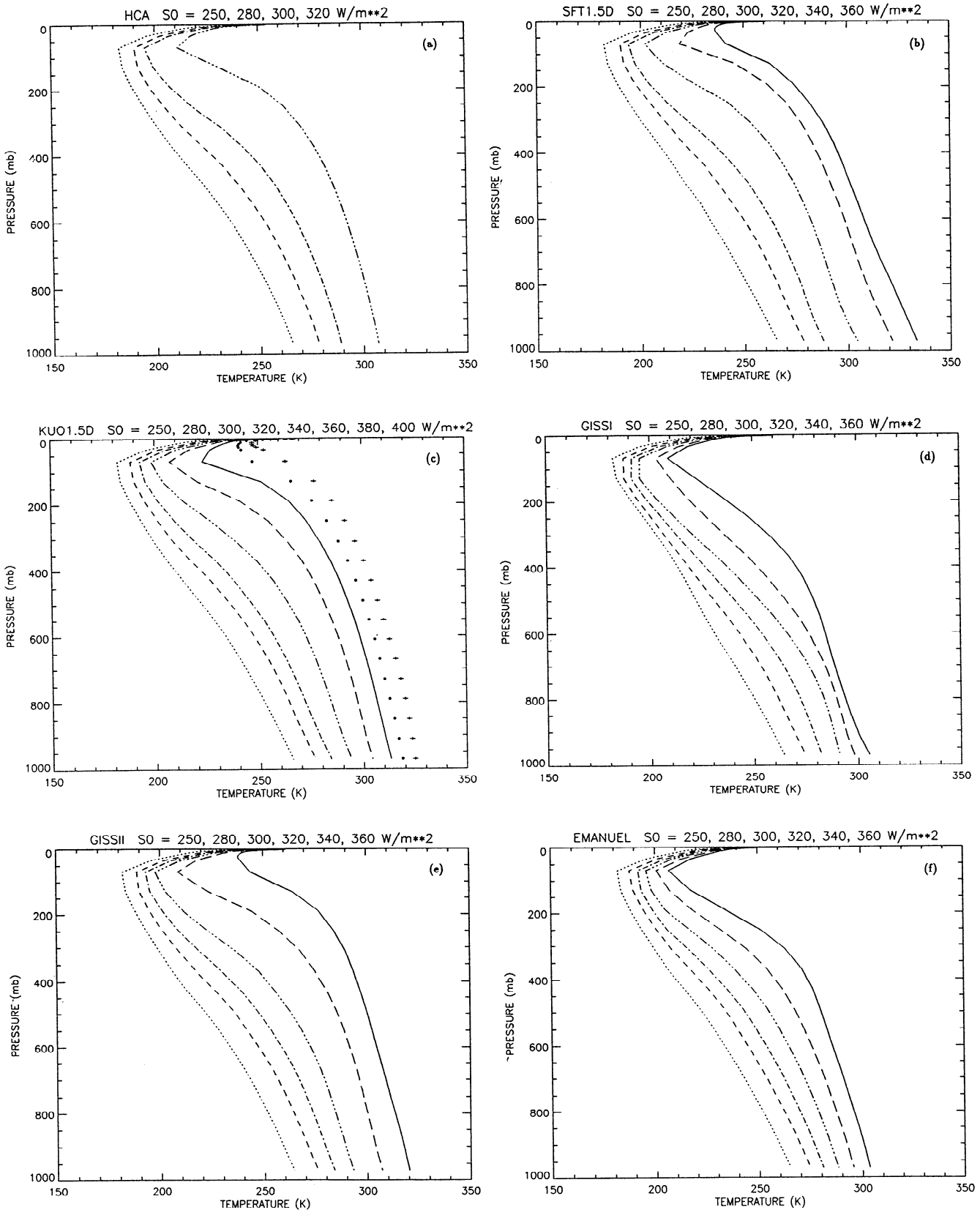


**Figure 7.** Temperature (K) profiles for various solar forcings (250 W $m^{-2}$, dotted line; 280 W $m^{-2}$, short-dashed line; 300 W $m^{-2}$, dotted-dashed line; 320 W $m^{-2}$, three-dotted-dashed line; 340 W $m^{-2}$, dashed line; 360 W $m^{-2}$, solid line; 380 W $m^{-2}$, large-dots, 400 W $m^{-2}$, crosses.) for (a) the hard convective adjustment (HCA) scheme; (b) the soft convective adjustment (SCA1.5D) scheme; (c) the kuo (Kuo1.5D) scheme; (d) the early GISS model (GISS1) scheme; (e) the GISS model II (GISS2) scheme; (f) the Emanuel scheme. Clear sky conditions and interactive water vapor are assumed for the computation of the radiative fluxes.

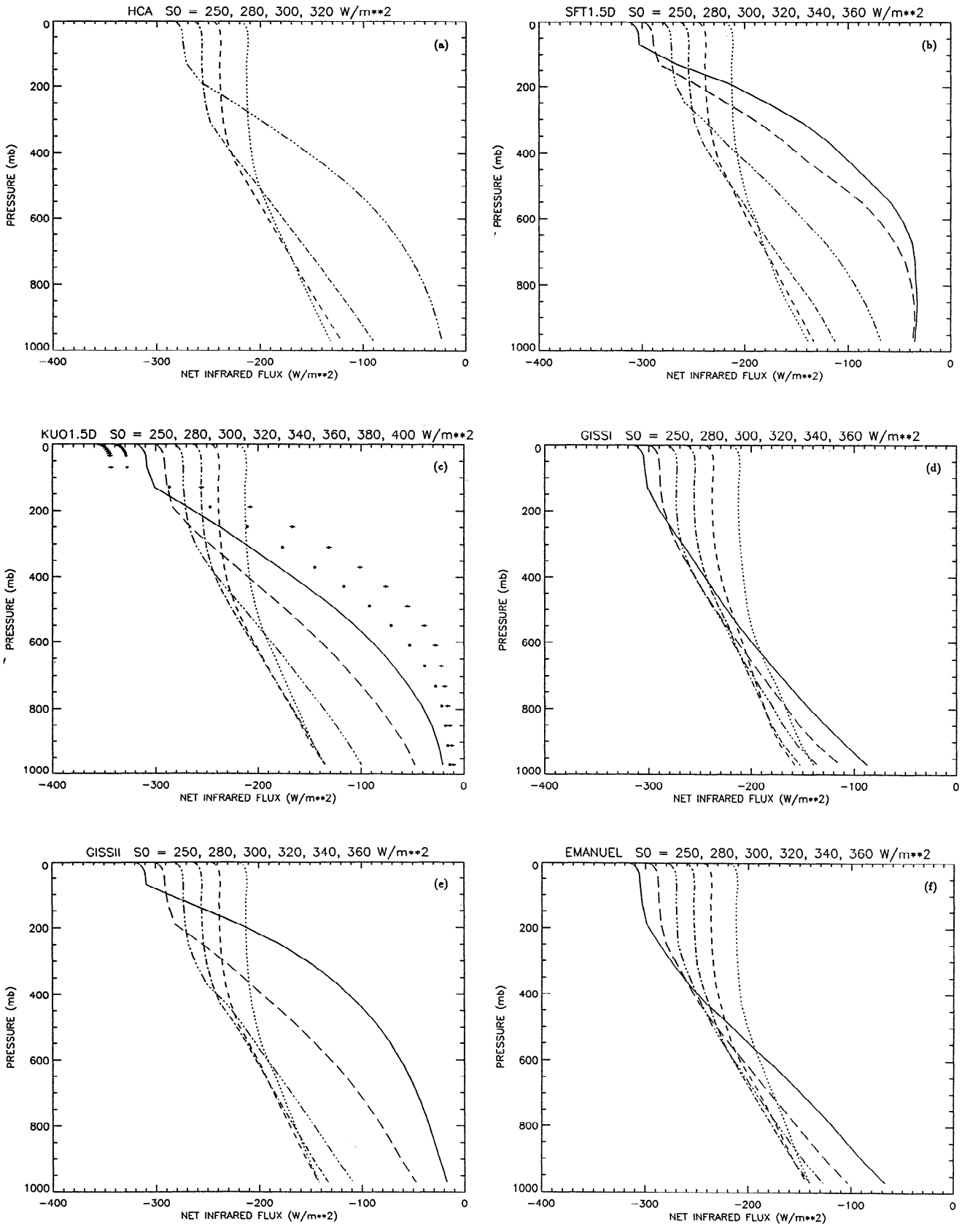


**Figure 8.** Net infrared flux (W $m^{-2}$) profiles for various solar forcings (250 W $m^{-2}$, dotted line; 280 W $m^{-2}$, short-dashed line; 300 W $m^{-2}$, dotted-dashed line; 320 W $m^{-2}$, three-dotted-dashed line; 340 W $m^{-2}$, dashed line; 360 W $m^{-2}$, solid line; 380 W $m^{-2}$, large-dots, 400 W $m^{-2}$, crosses.) for (a) the HCA scheme; (b) the SCA1.5D scheme; (c) the Kuo1.5D scheme; (d) the GISS1 scheme; (e) for GISS2 scheme; (f) the Emanuel scheme. Clear sky conditions and interactive water vapor are assumed for the computation of the radiative fluxes.

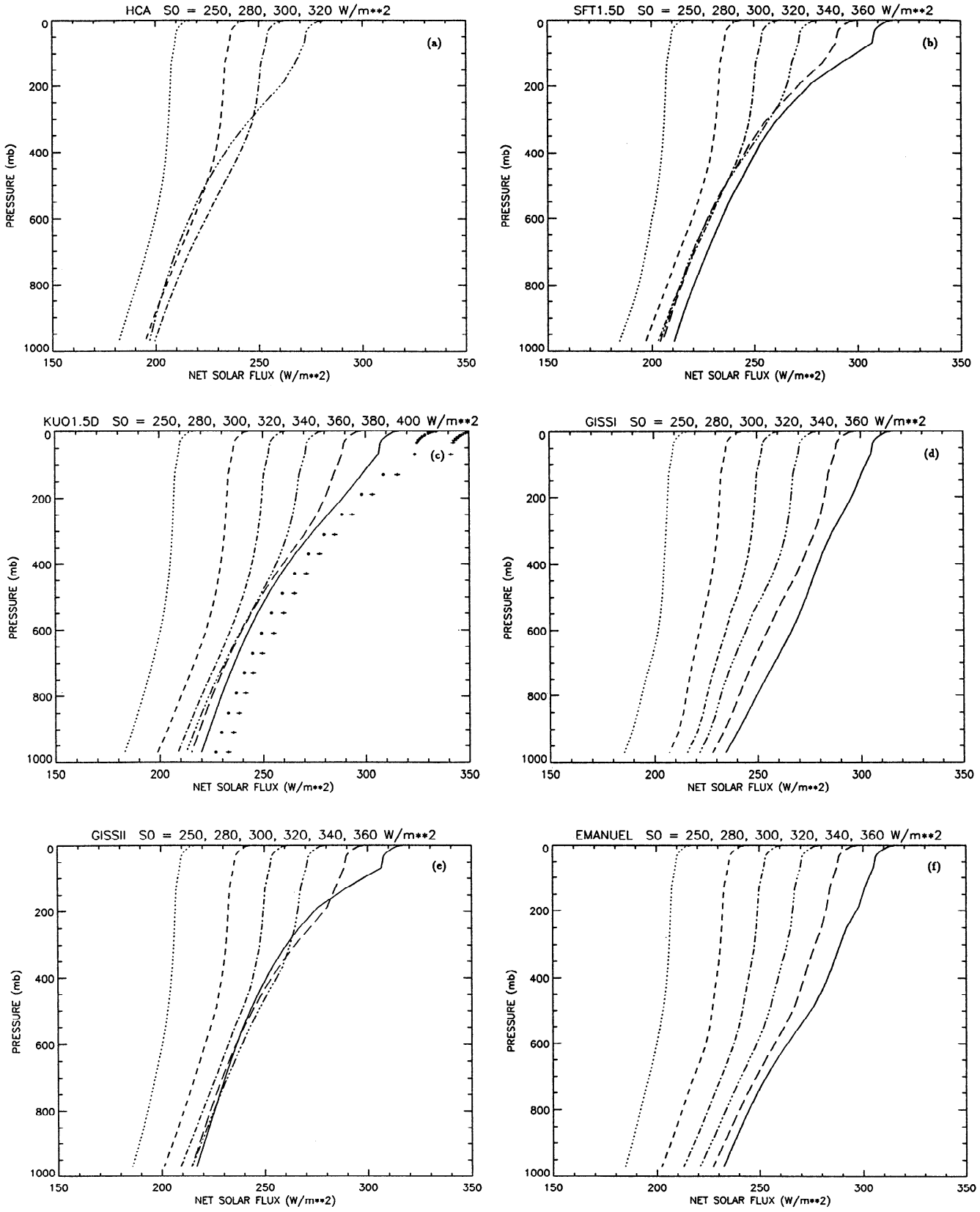


**Figure 9.** Net solar flux (W $m^{-2}$) profiles for various solar forcings (250 W $m^{-2}$, dotted line; 280 W $m^{-2}$, short-dashed line; 300 W $m^{-2}$, dotted-dashed line; 320 W $m^{-2}$, three-dotted-dashed line; 340 W $m^{-2}$, dashed line; 360 W $m^{-2}$, solid line; 380 W $m^{-2}$, large-dots, 400 W $m^{-2}$, crosses.) for(a) the HCA scheme; (b) the SCA1.5D scheme; (c) the Kuo1.5D scheme; (d) the GISS1 scheme; (e) the GISS2 scheme; (f) the Emanuel scheme. Clear sky conditions and interactive water vapor are assumed for the computation of the radiative fluxes.

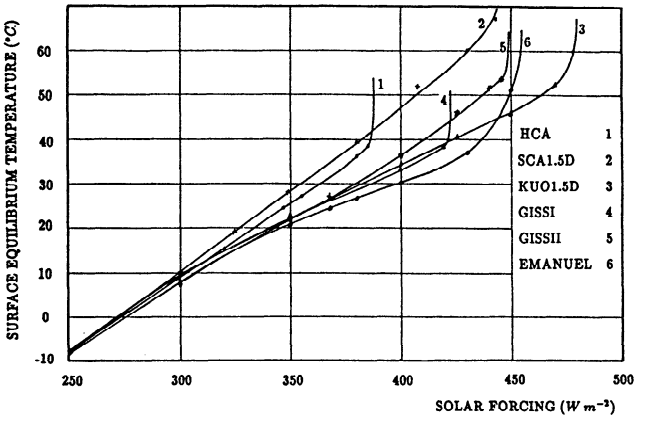


**Figure 10.** The surface temperature (° C) in radiative-convective equilibrium obtained with the various cumulus convection schemes. Fixed cloud cover and interactive water vapor are assumed for the computation of the radiative fluxes.

schemes, the equilibrium lower troposphere obtained in all experiments becomes opaque to infrared radiation as the solar fluxes increase (the net infrared flux approximates zero). As explained in section 5, the increase in the atmosphere's opacity is abrupt for the experiments with the GISS1 and Emanuel schemes and, to a lesser extent, for the experiments with the GISS2 scheme.

### 3.2. Experiments With Fixed Cloud Cover

Here, we briefly present the results of experiments similar to those presented in section 3.1 but with fixed cloud cover included in the computation of the radiative fluxes, as shown in part 1 [*Rennó et al.*, 1994]. Figure 10 shows the equilibrium surface temperature as a function of the solar forcing. The surface temperature is now less sensitive to the cumulus parameterization scheme.

The runaway greenhouse is still very sensitive to the cumulus parameterization scheme, but now it occurs for larger values of the forcing. The critical solar forcing is different for each one of the cumulus convection schemes tested. The HCA scheme presents the lowest critical solar forcing, 388 W $m^{-2}$; followed by the Emanuel scheme, 405 W $m^{-2}$; the GISS1 scheme, 423 W $m^{-2}$; the SCA1.5D scheme, 445 W $m^{-2}$; the GISS2 scheme, 450 W $m^{-2}$; and, finally, the Kuo1.5D scheme, 480 W $m^{-2}$.

## 4. Breakdown of the Radiative-Convective Equilibria

In this section we examine the behavior of the various cumulus convection schemes for supercritical solar forcing. The effects of clouds on the radiative fluxes are not included in the experiments discussed in this section. First, we look into the behavior of the model with the HCA scheme. Figure 11 shows a plot of the time

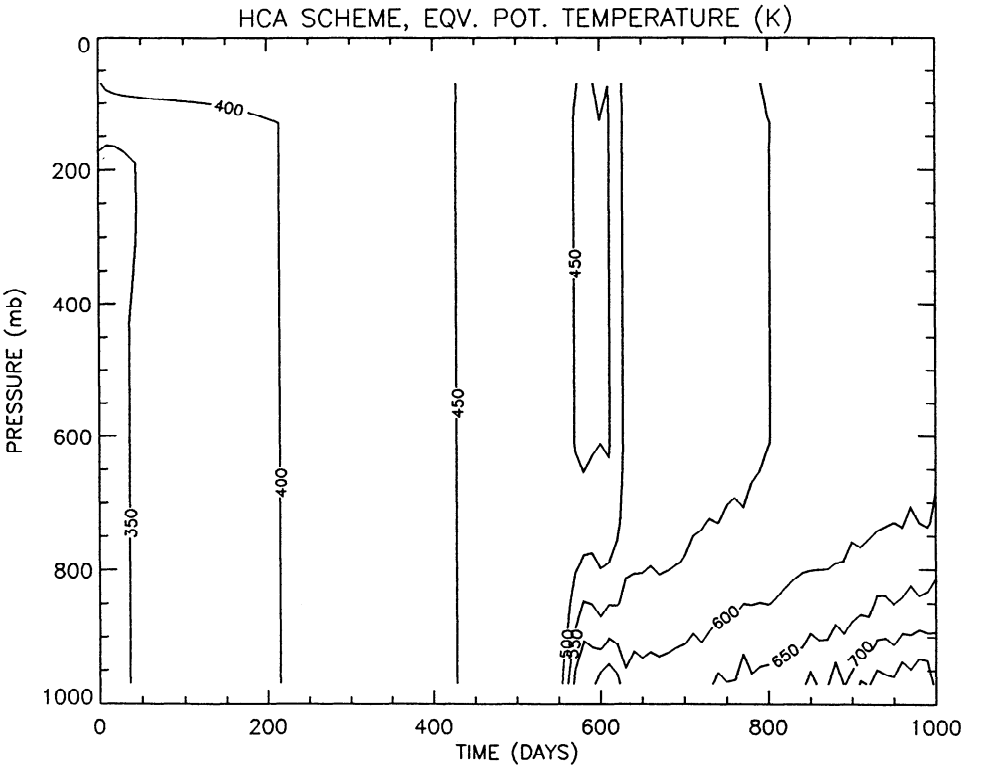


**Figure 11.** Time (days) evolution of the vertical profile of equivalent potential temperature (K) for the HCA scheme with supercritical solar forcing. The values plotted are averaged over the preceding 10 days of integration. Clear sky conditions and interactive water vapor are assumed for the computation of the radiative fluxes.

series of equivalent potential temperature throughout the model's atmosphere, while Figure 12 shows a similar plot but for the water vapor mixing ratio. From the beginning of the integration at time zero, up to about day 500, we observe a smooth increase in the equivalent potential temperature and water vapor mixing ratio throughout the model's atmosphere. During this period the convective layer is saturated and has a moist adiabatic temperature profile (the equivalent potential temperature is constant). Just after day 500 the lower troposphere becomes opaque to infrared radiation, causing all the radiative cooling to move to the middle-upper troposphere. The lower troposphere temperature increases steadly, but it is no longer kept saturated (because the rate of increase of the water vapor mixing ratio is barely strong enough to keep up with the increase in temperature). Since the lower troposphere is no longer kept saturated, instability is released only at the few time steps in which saturation occurs. At those times, bursts of convection produce very large precipitation events, as shown in Figure 13. Figure 14 shows a time series of the surface temperature in which it is interesting to note the sharp jump in the surface temperature when the atmosphere becomes opaque, at around day 600. Figures 15 and 16 show the equivalent potential temperature and the relative humidity profiles, respectively, at days 500 and 700. At day 500 the atmosphere is saturated and the equivalent potential temperature is constant throughout the troposphere. At day 700 there is not only a large increase in the equivalent potential temperature of the lower atmosphere but also a decrease in the middle-upper troposphere. The lower troposphere is no longer saturated.

Now, we look into the behavior of the model for supercritical solar forcing with the SCA1.5D and Kuo1.5D schemes. Figure 17 shows a plot of the time series of the equivalent potential temperature profile throughout the model's atmosphere, while Figure 18 shows a similar plot but for the water vapor mixing ratio. Both schemes produce a smooth transition to the runaway greenhouse. The SCA1.5D scheme produces a moist and unstable atmosphere when the runaway greenhouse is approached. The temperature and moisture of the lower troposphere increase steadly when it becomes opaque to infrared radiation, and moist convection is no longer able to keep a moist neutral atmosphere. The Kuo1.5D scheme produces a large temperature gradient in a transition layer between an unstable and moist lower troposphere and a neutral and dry upper troposphere. The dry upper atmosphere is due to a strong compensating subsidence at the layers of maximum convective heating.

The behavior of the GISS1, GISS2, and Emanuel schemes when the runaway greenhouse occurs is shown by the time series of equivalent potential temperature and water vapor mixing ratio profiles throughout the model's atmosphere (Figures 19 and 20). For the GISS1 and Emanuel schemes the runaway greenhouse is rapid. It is rapid because of a positive feedback generated by the interaction of the infrared radiation flux with detrained water vapor at the level of neutral buoyancy. The increase in the water vapor content at the detrainment level produces an increase in the radiative cooling

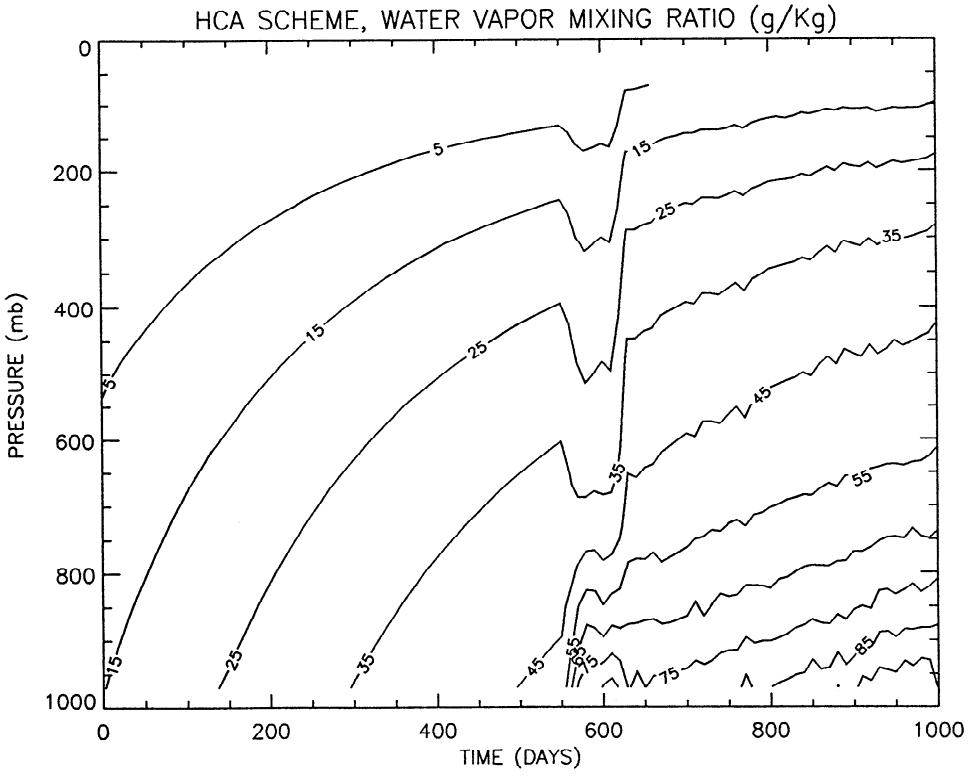


**Figure 12.** Same as in Figure (11) but for the water vapor mixing ratio.

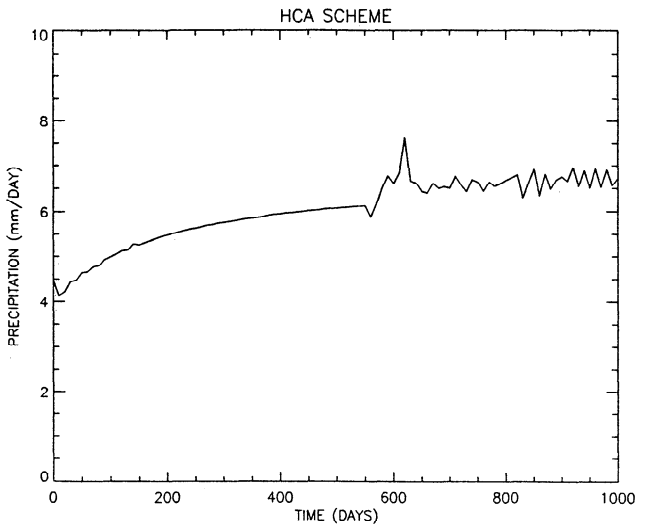


**Figure 13.** Time (days) evolution of precipitation (mm day$^{-1}$) for the HCA scheme with supercritical solar forcing. The values plotted are averaged over the preceding 10 days of integration. Clear sky conditions and interactive water vapor are assumed for the computation of the radiative fluxes.

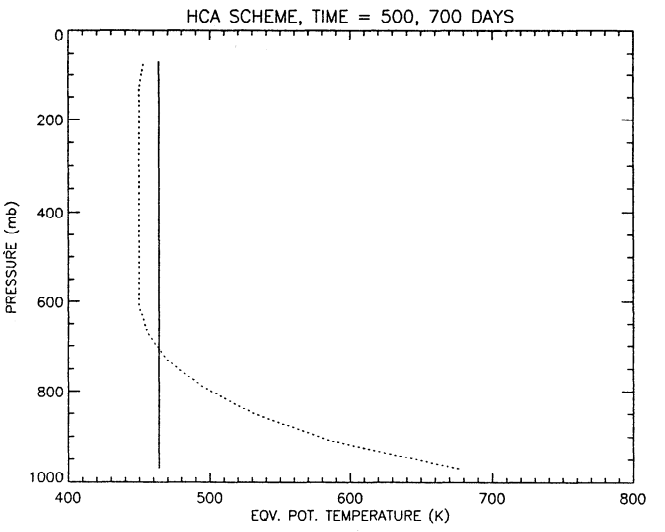


**Figure 15.** Vertical profile of equivalent potential temperature for the HCA scheme, averaged over the preceding 10 days of integration at day 500 (solid line) and day 700 (dotted line).

at this layer and a decrease in the radiative cooling of the lower layers (a greenhouse effect). The greenhouse effect produces an increase in the surface temperature and, therefore moisture, which in turn leads to an increase in the convective moisture flux. The increase in the convective moisture flux and in the radiative cooling at the upper layers leads to an increase in the detrainment of water vapor at the layer of neutral buoyancy. This increase in the detrainment of moisture feeds back on the process causing a rapid evolution when the moisture content of the detrainment layer is high enough to produce a substantial effect in the infrared radiation flux. When this feedback sets in, the atmosphere's temperature and moisture increase up to a point where it becomes opaque to infrared radiation, and then the "classical" runaway greenhouse takes over (i.e., the atmosphere's emission of infrared radiation reaches the Simpson-Komabayasi-Ingersoll limit).

## 5. Sensitivity of the Runaway Greenhouse to the Precipitation Efficiency

In this section we use the *Emanuel* [1991] cumulus convection scheme to assess the sensitivity of the run-

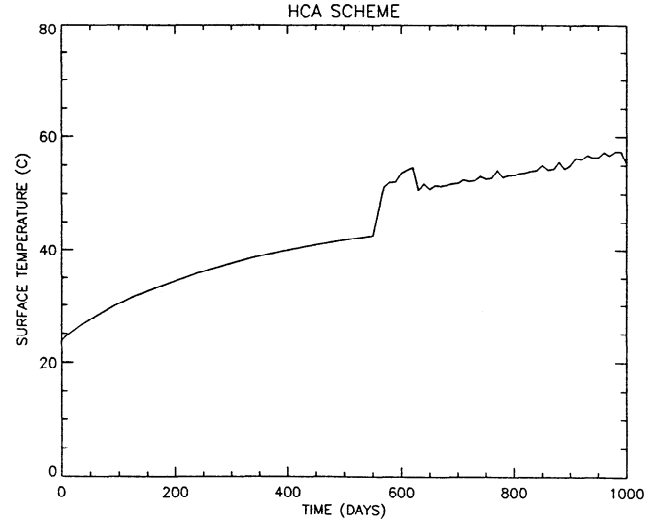


**Figure 14.** Same as in Figure (13) but for the surface temperature.

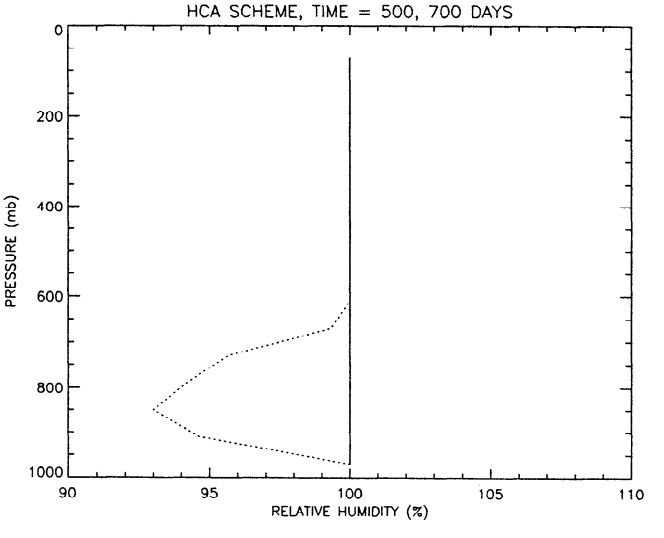


**Figure 16.** Same as in Figure (15) but for relative humidity at day 500 (solid line) and day 700 (dotted line).

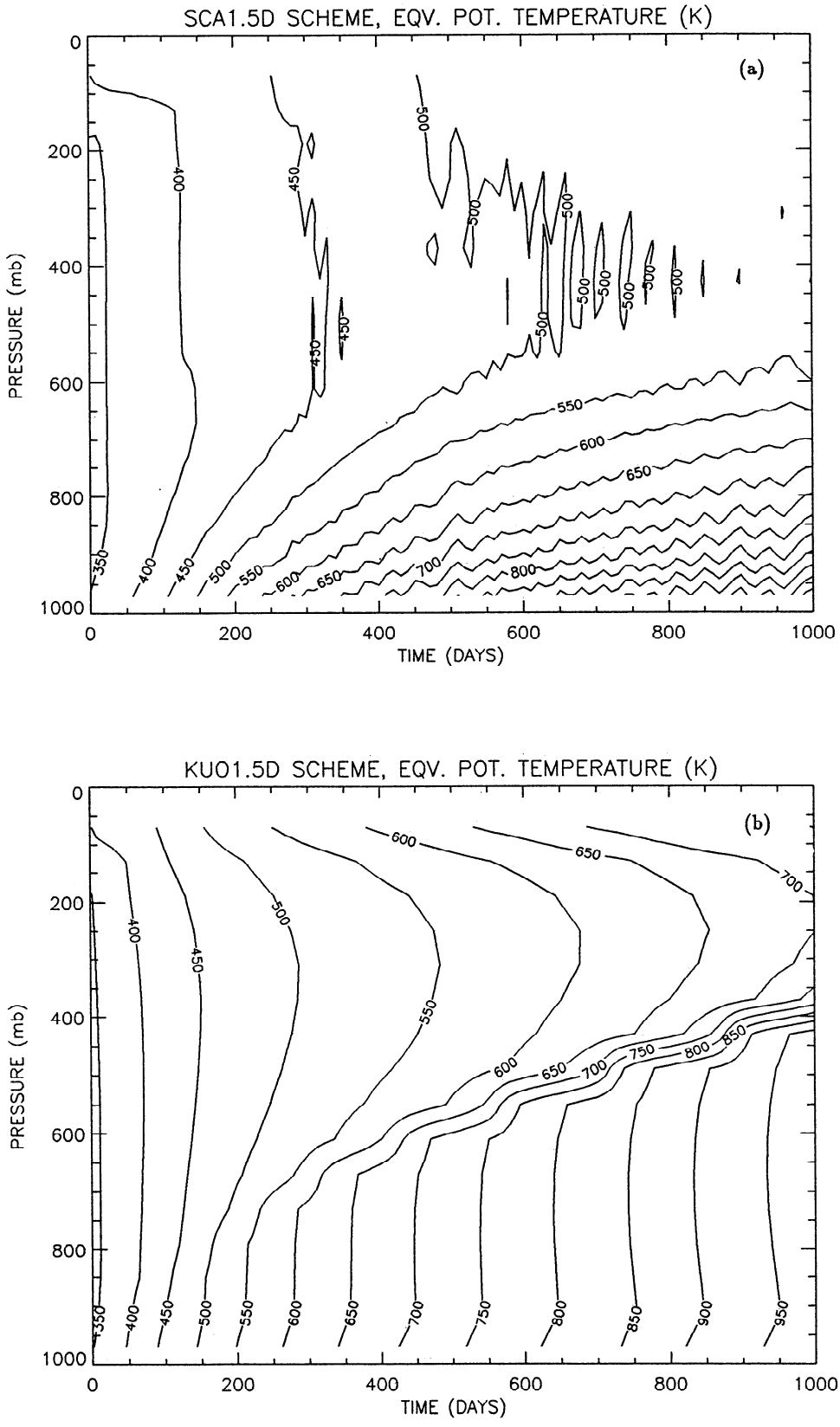


**Figure 17.** Same as in Figure (11) but for (a) the SCA1.5D scheme and (b) the Kuo1.5D scheme.

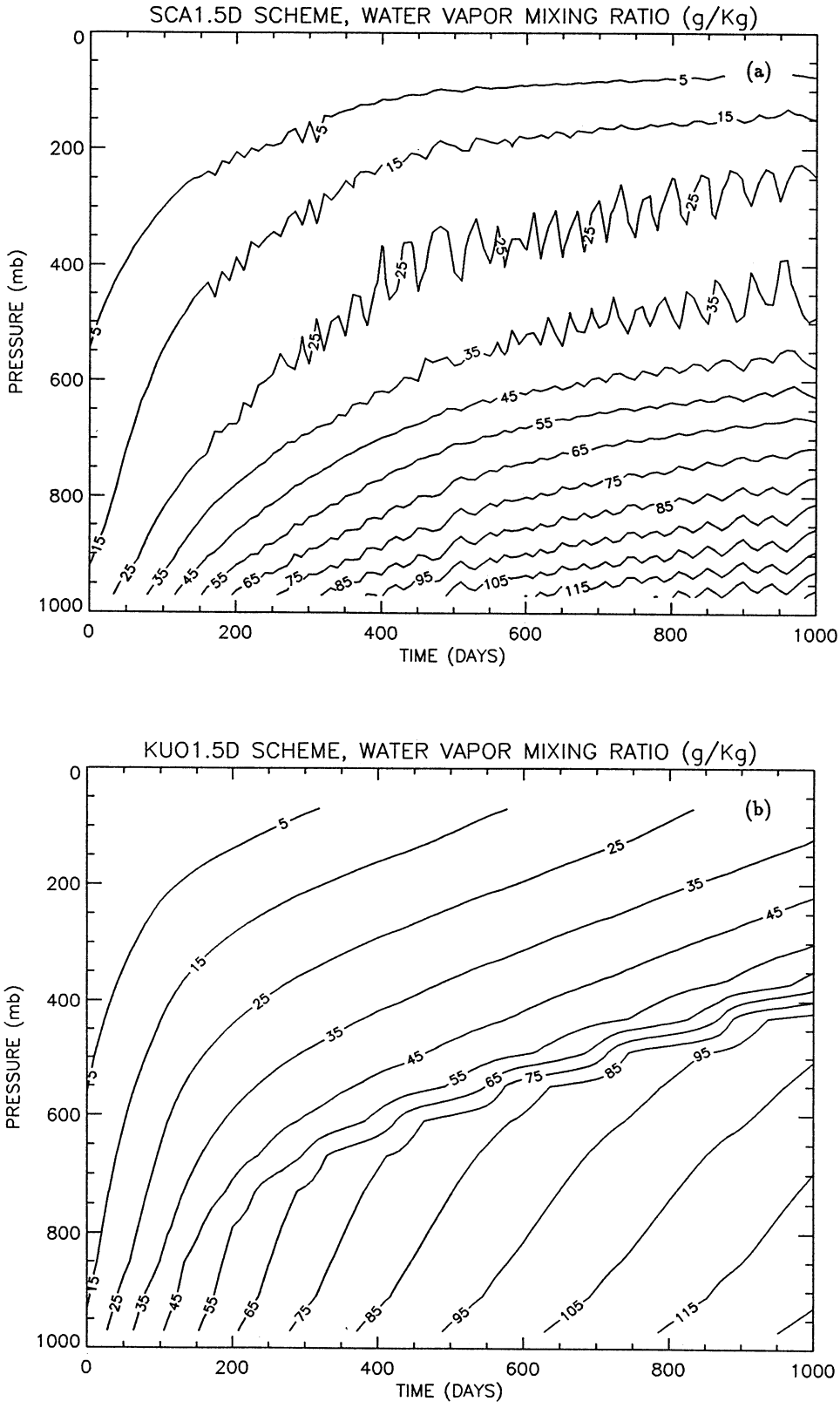


**Figure 18.** Same as in Figure (11) but for water vapor mixing ratio and for (a) the SCA1.5D scheme and (b) the Kuo1.5D scheme.

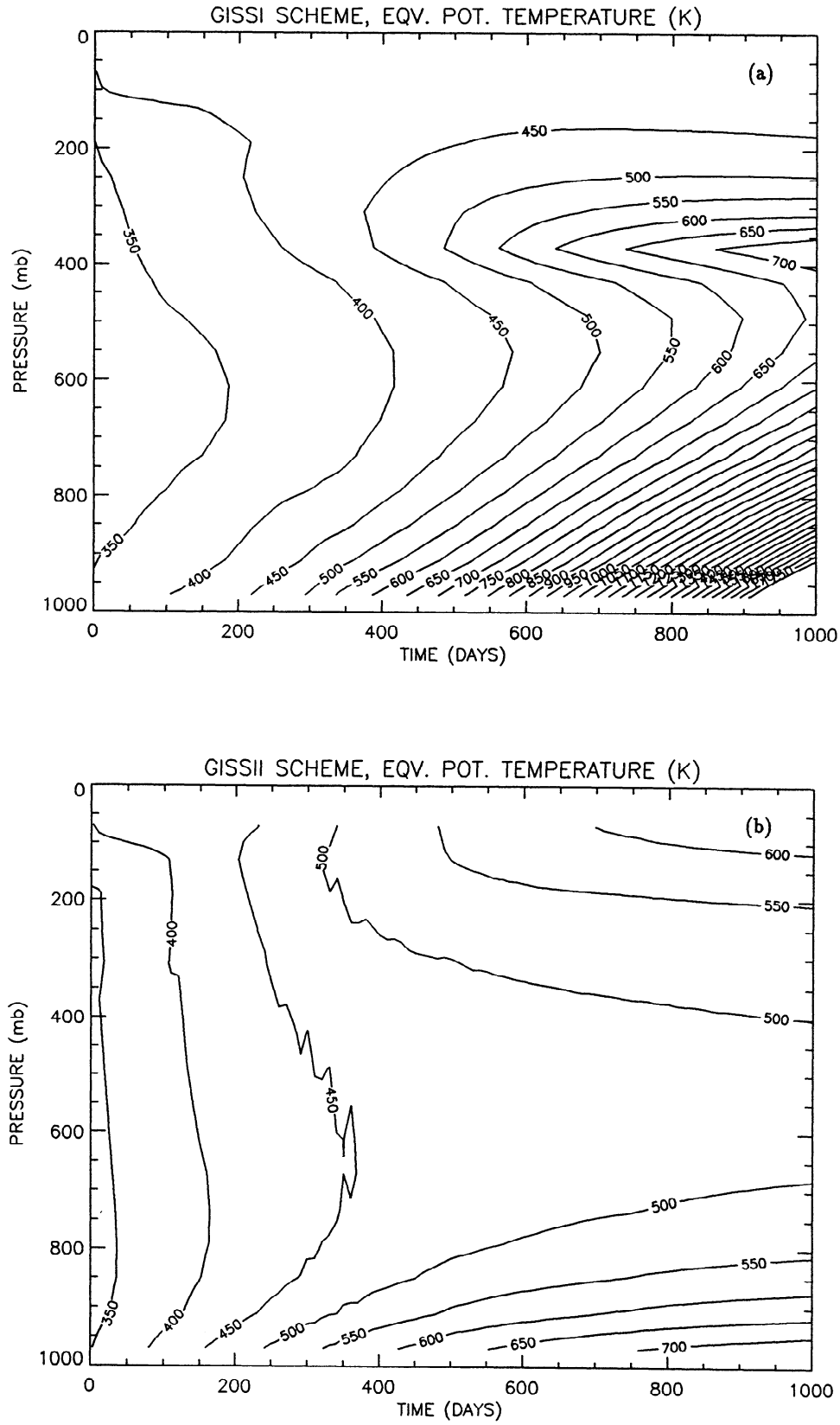


**Figure 19.** Same as in Figure (11) but for (a) the GISS1 scheme, (b) the GISS2 scheme, and (c) the Emanuel scheme.

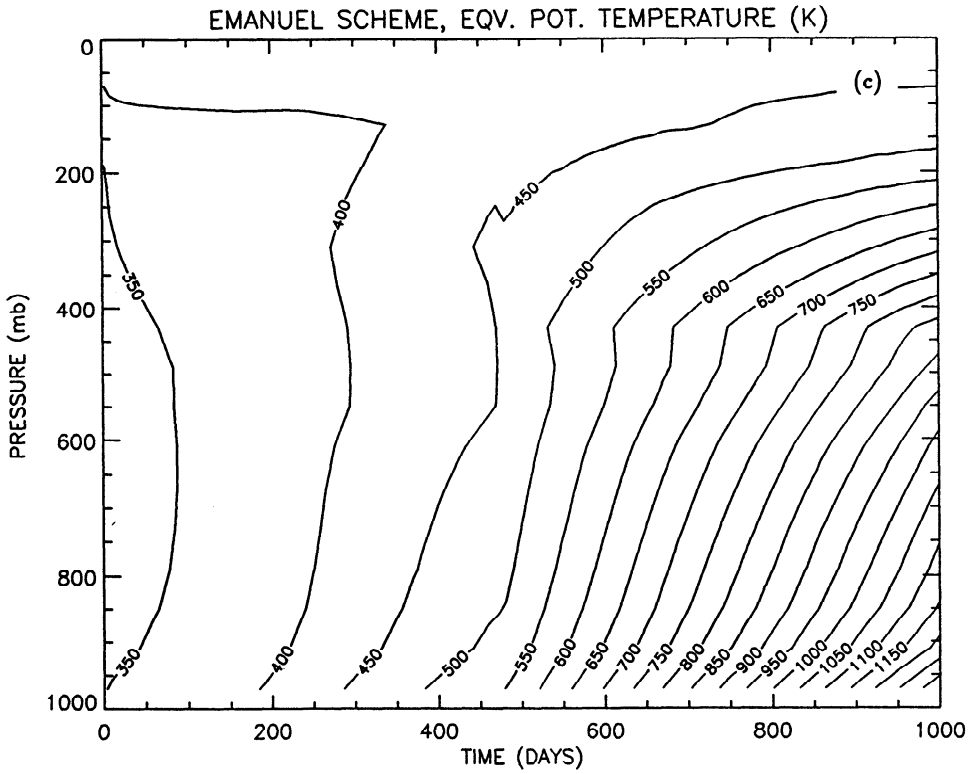


**Figure 19.** (Continued)

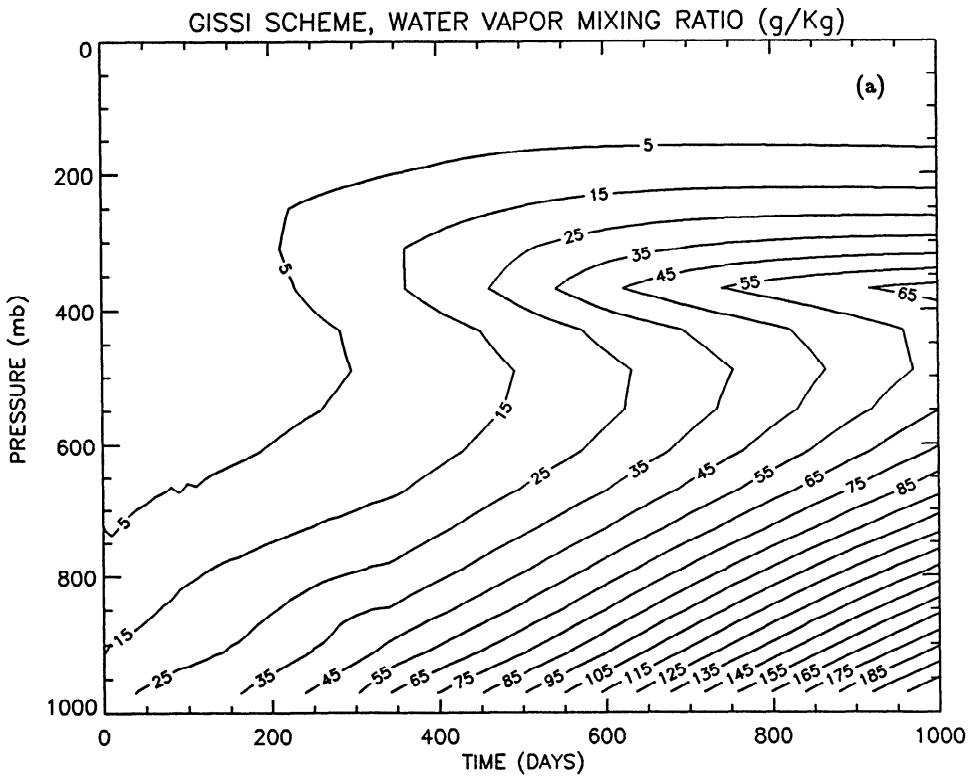


**Figure 20.** Same as in Figure (11) but for water vapor mixing ratio and for (a) the GISS1 scheme, (b) the GISS2 scheme, and (c) the Emanuel scheme.

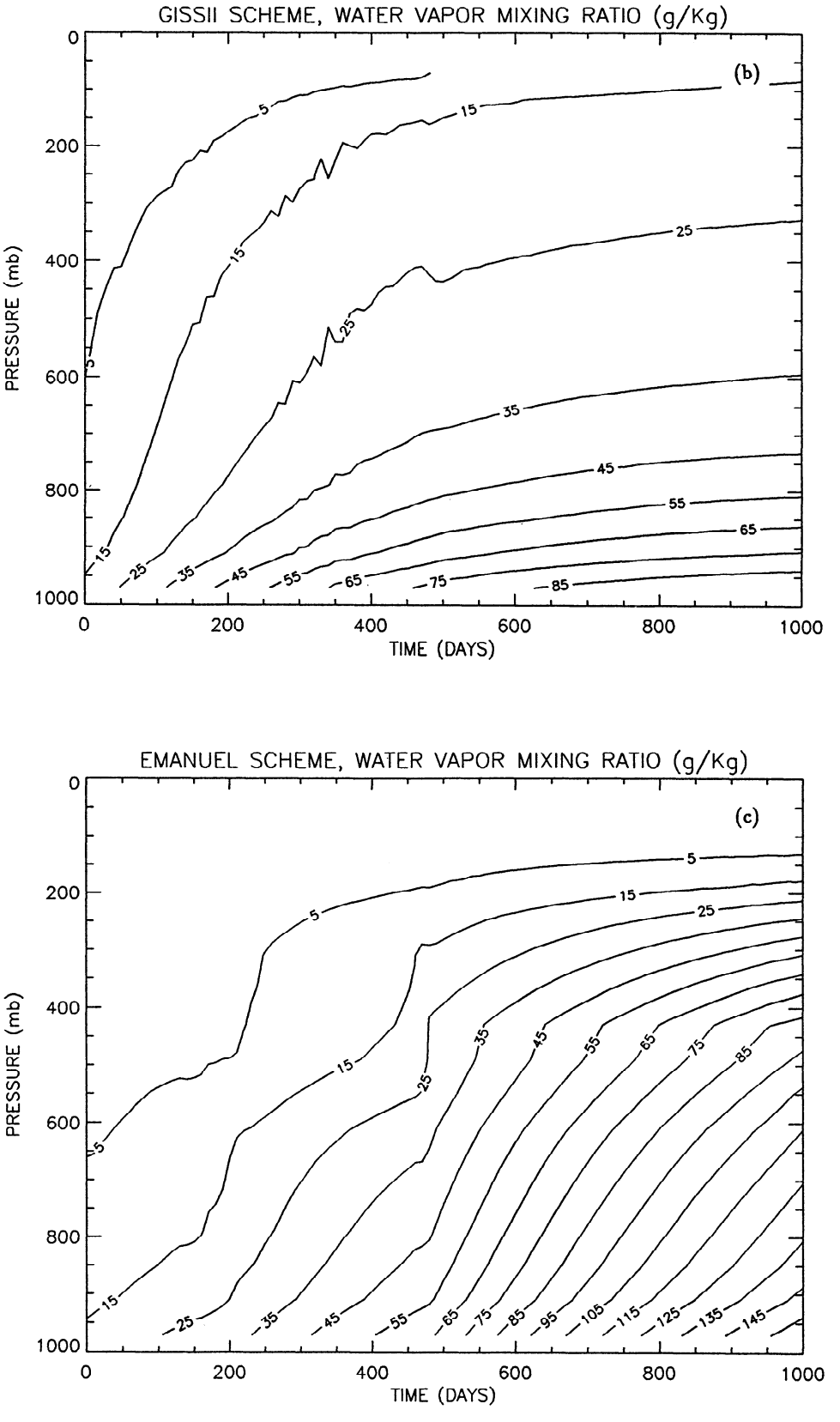


**Figure 20.** (Continued)

away greenhouse to the precipitation efficiency. The precipitation efficiency parameter in the calculations already described was computed as follows:

$$\epsilon_i = \begin{cases} 0, & p_{\rm icb} - p_i < PB_{\rm crit} \\ \frac{p_{\rm icb} - p_i - PB_{\rm crit}}{PT_{\rm crit} - PB_{\rm crit}}, & PB_{\rm crit} < p_{\rm icb} - p_i < PT_{\rm crit} \\ 1, & p_{\rm icb} - p_i > PT_{\rm crit}, \end{cases} \quad (3)$$

where $p_{\rm icb}$ is the cloud base pressure level and $PB_{\rm crit}$ and $PT_{\rm crit}$ are, respectively, the critical draft thicknesses below which the precipitation efficiencies, $\epsilon_i$, are assumed to be zero and above which they are taken to be the unity. In the previous sections, $PB_{\rm crit}$ was set to 150 mbar, and $PT_{\rm crit}$ was set to 500 mbar. The results presented in this section are for constant precipitation efficiencies (throughout the convecting layers).

Figure 21 shows the surface equilibrium temperature obtained with the Emanuel scheme with low and high precipitation efficiency as a function of the solar forcing. The critical value of the solar forcing depends strongly on the precipitation efficiency. For a small precipitation efficiency ($\epsilon_i = 0.1$) the atmosphere is very unstable to changes in the solar forcing and the runaway greenhouse occurs for solar forcing around 324 W m$^{-2}$. This happens because the water vapor content of this atmosphere is very high due to the detrainment of a large amount of water vapor from low precipitation-efficiency clouds. For a large precipitation efficiency ($\epsilon_i = 1.0$) the atmosphere is less unstable to changes in the solar forcing and the runaway greenhouse occurs for solar forcing around 415 W m$^{-2}$. This happens because the equilibrium atmosphere is relatively dry and saturation occurs only at the neutral buoyancy level. In this case, the runaway greenhouse is rapid because of the positive feedback described in section 5. The rapid runaway does not occur in the low precipitation efficiency case because, there, the level of maximum radiative cooling rises gradually (there is a large detrainment of moisture throughout the convective layer). In the high precipitation efficiency case, it jumps from the low troposphere to the upper troposphere (since the middle troposphere is very dry).

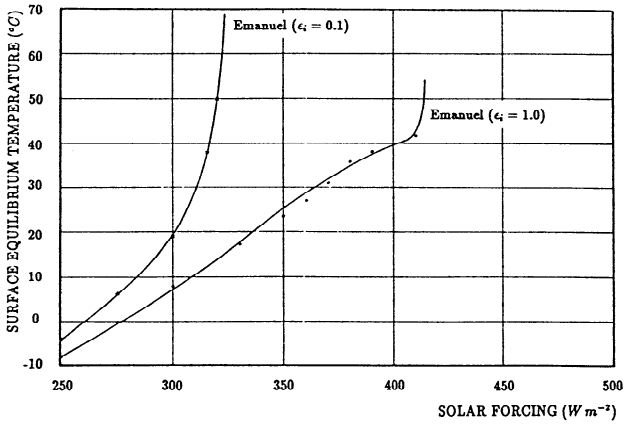


**Figure 21.** The surface temperature in radiative-convective equilibrium obtained with the *Emanuel* [1991] cumulus convection scheme with small precipitation efficiency, $\epsilon_i = 0.1$, and with high precipitation efficiency, $\epsilon_i = 1.0$.

## 6. Implications for the Climates of Moist Planets

*Pollack* [1971] determined that the critical solar forcing, in order for a runaway greenhouse to occur, in a pure $H_2O$ atmosphere with 50% cloud cover, is between 1.4 and 2.0 times the present terrestrial value, depending on the assumed relative humidity profile. *Kasting et al.* [1984] studied the response of a cloudless, saturated atmosphere, with a moist adiabatic temperature lapse rate, to large changes in the solar forcing. When the water vapor continuum absorption outside of the 8 to 12-$\mu$m window region was negleted, they predicted a monotonic increase in the surface equilibrium temperature, from $-1°$ to 111° C as the solar flux increased from 0.81 to 1.45 times the present value for the Earth. In this case, a runaway greenhouse did not occur. However, when *Kasting et al.* [1984] crudely included the water vapor continuum absorption outside of the 8 to 12-$\mu$m window region the critical solar forcing for runaway greenhouse to occur was about 1.16 times the present value for the Earth. The radiation parameterization scheme used in our model includes the the water vapor continuum absorption outside of the 8 to 12-$\mu$m window region [*Chou et al.*, 1991].

The models of *Pollack* [1971] and *Kasting et al.* [1984] do not clearly predict a runaway greenhouse for Venus, since the present solar forcing at the Venus orbit is 1.91 times the present value for the Earth, and it was about 1.34 times at the time of its formation, at about 4.5 billion years ago [*Newkirk*, 1980]. Our results show that the critical solar forcing for a runaway greenhouse to occur in a moist planet is also very sensitive to the parameterization of cumulus convection as well as to the cloud microphysical processes.

Taking the solar forcing as the arbitrary parameter, we compute $F_0$, the solar forcing necessary for an equilibrium surface temperature equal to 15° C. Then, we compute the critical solar forcing for runaway greenhouse to occur, $F_R$. The ratio $F_R/F_0$ is a rough estimative of how much the present terrestrial solar forcing must be increased in order for a runaway greenhouse to occur (Tables 2 and 3).

When clear sky conditions are used in the computation of the radiative fluxes, our model predicts that the ratio $F_R/F_0$ is between 1.10 and 1.41 (see Table 1). It is the smallest for the Emanuel scheme with low precipitation efficiencies and the largest for the Kuo1.5D scheme. When fixed cloud cover is used (see Table 2), it is the smallest for the HCA scheme, 1.22, and the largest for the Kuo1.5D scheme, 1.49. Therefore our model undoubtedly predicts a runaway greenhouse for Venus with its present value of the solar forcing, but this may not hold for 4.5 billion years ago.

**Table 2.** Solar Forcing Parameters for Earth-like Conditions and for Runaway Greenhouse to Occur.

| Scheme | Clear Sky Conditions | | |
|---|---|---|---|
| | $F_o$ | $F_R$ | $F_R/F_o$ |
| HCA | 291 | 332 | 1.14 |
| SCA1.5D | 294 | 373 | 1.27 |
| Kuo1.5D | 301 | 424 | 1.41 |
| GISS1 | 309 | 363 | 1.17 |
| GISS2 | 304 | 378 | 1.24 |
| Emanuel (STD) | 312 | 368 | 1.18 |
| Emanuel ($\epsilon = 0.1$) | 293 | 324 | 1.10 |
| Emanuel ($\epsilon = 1.0$) | 321 | 415 | 1.29 |

HCA, hard convective adjustment scheme; SCA1.5D, soft convective adjustment scheme; Kuo1.5D, kuo scheme; GISS1, early GISS model scheme; GISS2, GISS model II scheme; Emanuel (STD), Emanuel scheme with the standard set of parameters (section 5). Clear sky conditions are used in the computation of the radiation fluxes.

Finally, we should emphasize that the results of our model are not directly applicable to other planets, since Earth-like conditions were assumed (e.g., atmosphere's composition and surface albedo).

## 7. Conclusion

We showed that the various cumulus convection schemes tested produce a runaway greenhouse for relatively small values of the solar forcing. For fixed cloud cover conditions, the critical solar forcing in order for a runaway greenhouse to occur is between approximately 1.22 and 1.49 times the current value for the Earth. We also showed that the runaway greenhouse can occur very rapidly in the experiments with the mass flux schemes but only gradualy in the experiments with the adjustment schemes.

Our results are in contradiction to those obtained by *Sarachik* [1978], who argued that the equilibrium surface temperature is relatively insensitive to changes in the solar forcing. He pointed out that increases in solar flux are compensated by additional evaporation. However, since he used a simple Newtonian parameterization for the computation of radiative cooling, his model failed to account for a decrease in the cooling of the planetary boundary layer due to an increase in the water vapor content of the atmosphere's interior. Furthermore, his model failed to account for the crucial interactions of infrared radiative fluxes with the moisture content of the upper layers of the convective region.

**Table 3.** Same as Table 2 but for Fixed Cloud Cover

| Scheme | Fixed Cloud Cover | | |
|---|---|---|---|
| | $F_o$ | $F_R$ | $F_R/F_o$ |
| HCA | 319 | 388 | 1.22 |
| SCA1.5D | 315 | 445 | 1.41 |
| Kuo1.5D | 322 | 480 | 1.49 |
| GISS1 | 322 | 323 | 1.31 |
| GISS2 | 326 | 450 | 1.38 |
| Emanuel (STD) | 327 | 460 | 1.41 |

Our results are also in contradiction with those obtained by *Lindzen et al.* [1982] who challenged the validity of the runaway greenhouse by arguing that a "physically based" convection scheme inhibts it through the adjustments in the temperature lapse rate. In fact, the runaway greenhouse in their model was inhibited by two major approximations: first, by the assumption of a fixed climatological profile of relative humidity, probably not valid for large changes in the solar forcing; and second, by the treatment of infrared radiation based on the *Rodgers* [1968] emissivity formulation, which does not account for the important water vapor continuum absorption [*Kasting et al.*, 1984]. As shown in Figure 1, the runaway greenhouse is also inhibited in our model when the relative humidity profile is fixed at climatological values for the Earth.

Finally, it is important to understand the limitations of our study. One major drawback is that cloud-radiation feedbacks are not well known at this time. Since clouds have a large impact on radiative fluxes, they are potentially a key factor in determining whether or not a runaway greenhouse will ever occur in a moist atmosphere. Another problem is uncertainties in the parameterization of the water vapor continuum absorption of infrared radiation outside the 8 to 12-$\mu$m window region. Although it has little effect on the climate equilibrium for present conditions on Earth, it has a very large impact on the effects of large increases in the solar forcing [*Kasting et al.*, 1984].

**Acknowledgments.** We would like to thank Drs. W. Ridgway and M. -D. Chou of NASA/GSFC for providing the radiation code and pronptly answering our numerous questions. We also would like to thank M. C. Lemos for reading the manuscript more than once.

## References

Arakawa, A., Parameterization of cumulus convection, in *Proceedings of WMO/IUGG Symposium of Numerical Weather Prediction*, pp. 1-6, Japan Meteorological Society, Tokyo, 1969.

Arakawa, A. and W. H. Schubert, Interaction of a cumulus cloud ensemble with the large-scale environment, *J. Atmos. Sci., 31,* 674-701, 1974.

Asselin, R., Frequency filter for time integrations, *Mon. Weather Rev., 100,* 437-490, 1972.

Betts, A. K., Saturation point analysis of moist convective overturning, *J. Atmos. Sci., 39,* 1484-1505, 1982.

Betts, A. K., Mixing line analysis of clouds and cloudy boundary layers, *J. Atmos. Sci., 42,* 2751-2763, 1985.

Betts, A. K., and W. Ridgway, Coupling of the radiative, convective, and surface fluxes over the equatorial pacific, *J. Atmos. Sci., 45,* 522-536, 1988.

Chapman, S., The atmospheric height distribution of band-absorbed solar radiation, *Proc. Phys. Soc. London, 51,* 93, 1939.

Chou, M.-D., A solar radiation model for use in climate studies, *J. Atmos. Sci., 49,* 762-772, 1992.

Chou, M.-D., D. P. Krats, and W. Ridgway, Infrared radiation parameterization in numerical climate models, *J. Clim., 4,* 424-437, 1991.

Emanuel, K. A., A scheme for representing cumulus convection in large-scale models, *J. Atmos. Sci., 48,* 2313-2335, 1991.

Goody, R. M., and Y. L. Yung, *Atmospheric radiation, theoretical basis,* 2nd ed., 519 pp., Oxford University Press, New York, 1989.

Hansen, J., G. Russell, D. Rind, P. Stone, A. Lacis, S. Lebedeff, R. Ruedy, and L. Travis, Efficient three-dimensional global models for climate studies: Model I and II, *Mon. Weather Rev., 111,* 609-662, 1983.

Ingersoll, A. P., The runaway greenhouse: A history of water on Venus, *J. Atmos. Sci., 26,* 1191-1198, 1969.

Kasting, J. F., J. B. Pollack, and D. Crisp, Effects of high $CO_2$ levels on surface temperature and atmospheric oxidation state on the early Earth, *J. Atmos. Chem., 1,* 423-428, 1984.

Komabayasi, M., Discrete equilibrium temperatures of a hypothetical planet with the atmosphere and the hydrosphere of one component-two phase system under constant solar radiation, *J. Meteor. Soc. Japan, 45,* 137-138, 1967.

Kuo, H. L., Further studies of the parameterization of the influence of cumulus convection on large-scale flow, *J. Atmos. Sci., 31,* 1232-1240, 1974.

Lindzen, R. S., A. Y. Hou, and B. F. Farrel, The role of convective model choice in calculating the climate impact of doubling $CO_2$, *J. Atmos. Sci., 39,* 1189-1205, 1982.

Manabe, S., and Strickler, R. F., Thermal equilibrium of the atmosphere with a convective adjustment, *J. Atmos. Sci., 21,* 361-385, 1964.

Manabe, S., and J. Wetherald, R. T., Thermal equilibrium of the atmosphere with a given distribution of relative humidity, *J. Atmos. Sci., 24,* 241-259, 1967.

Manabe, S., J. Smagorinsky, and R. F. Strickler, Simulated climatology of a general circulation model with a hydrologic cycle, *Mon. Weather Rev., 93,* 769-798, 1965.

Manabe, S., R. J. Stouffer, M. J. Spelman, and K. Bryan, Transient response of a coupled ocean-atmosphere model to gradual changes of atmospheric $CO_2$, 1. Annual mean response, *J. Clim., 4,* 785-819, 1991.

McClatchey, R. A., R. W. Fenn, J. E. A. Selby, F. E. Volz, and J. S. Garing, Optical properties of the atmosphere, *Environ. Res. Pap. 411,* Air Force Cambridge Res. Lab., Hanscon Air Force Base, Mass., 1972.

Newkirk, G. Jr., Solar variability on time scales of $10^5$ years to $10^{9.6}$ years, in *Proceedings of the Conference of the Ancient Sun,* edited by R. O. Pepin, J. A. Eddy, and R. B. Merrill, Pergamon, New York, 1980.

Pollack, J. B., A nongray calculation of the runaway greenhouse: Implications for venus's past and present, *Icarus, 14,* 295-306, 1971.

Rennó, N. O., Cumulus convection parameterization and numerical modelling of moist atmospheres, *Ph.D. thesis, 297 pp., Mass. Inst. of Technol.,* Cambridge, 1992.

Rennó, N. O., K. A. Emanuel, and P. H. Stone, A radiative-convective model with an explicit hydrologic cycle, 1. Formulation and sensitivity to model parameters, *J. Geophys. Res., in press,* 1994.

Rodgers, C. D., Some extension and applications of the new random model for molecular band transmission, *Q. J. R. Meteorol. Soc., 94,* 99-102, 1968.

Sarachik, E. S., Tropical sea surface temperature: An interactive one-dimensional atmosphere ocean model, *Dyn. Atmos. Oceans, 2,* 455-469, 1978.

Simpson, G. C., Some studies in terrestrial radiation, *Mem. R. Meteorol. Soc., 2,* 16, 1927.

Somerville, R. C. J., P. H. Stone, M. Harlen, J. E. Hansen, J. S. Hogan, L. M. Druyan, G. Russell, A. A. Lacis, W. J. Quirk, and J. Tenenbaum, The GISS model of the global atmosphere, *J. Atmos. Sci., 31,* 84-117, 1974.

Stone, P. H., and J. Risbey, On the limitations of general circulation climate models, *Geophys. Res. Lett., 17,* 2173-2176, 1990.

K. A. Emanuel and P. H. Stone, Center for Meteorology and Physical Oceanography, Massachusetts Institute of Technology, Cambridge, MA 02139.

N. O. Rennó, Planetary Sciences, Mail Code 170-25, California Institute of Technology, Pasadena, CA 91125.

(Received March 10, 1993; revised February 8, 1994; accepted May 13, 1994.)